

RSC Advances



This is an *Accepted Manuscript*, which has been through the Royal Society of Chemistry peer review process and has been accepted for publication.

Accepted Manuscripts are published online shortly after acceptance, before technical editing, formatting and proof reading. Using this free service, authors can make their results available to the community, in citable form, before we publish the edited article. This *Accepted Manuscript* will be replaced by the edited, formatted and paginated article as soon as this is available.

You can find more information about *Accepted Manuscripts* in the [Information for Authors](#).

Please note that technical editing may introduce minor changes to the text and/or graphics, which may alter content. The journal's standard [Terms & Conditions](#) and the [Ethical guidelines](#) still apply. In no event shall the Royal Society of Chemistry be held responsible for any errors or omissions in this *Accepted Manuscript* or any consequences arising from the use of any information it contains.

Tuning structures and electron transport properties of ultrathin Cu nanowires by size and bending stress using DFT and DFTB methods

C. He¹, G. Liu¹, W.X. Zhang^{2*}, Z.Q. Shi^{1*}, S.L. Zhou¹

¹ *State Key Laboratory for Mechanical Behavior of Materials, School of Materials Science and Engineering, Xi'an Jiaotong University, Xi'an 710049, China*

² *School of Materials Science and Engineering, Chang'an University, Xi'an 710064, China*

Abstract

The electron transport properties of ultrathin Cu nanowires (NWs) with diameter of 0.2-1.0 nm under different bending stresses are reported for the future application in flexible displays and flexible solar cell. The density functional theory (DFT) and density-functional-based tight-binding (DFTB) approaches have been combined to systematically discover the ballistic transport and diffusive transport of ultrathin Cu NWs in the nanoscale. Our DFT calculations show that with the increasing of bending stress (f), the structures of both nonhelical and helical wires become disorder, then exhibit phase transition and eventually collapse. Therefore, the quantum conduction(G) are reduced. In addition, as the size of nanowires increases, the maximum bearable bending stress (f_c) reduces. f_c of a helical atomic strand is decided by its diameter, while f_c of a nonhelical atomic strand is decided by the area of the cross section. Our DFTB calculations reveal that the intermediary atoms are the highlight to form the loop between two electrodes and implement diffusion transport. Among the seven structures, the 6-1b exhibits the best properties by comprehensively considering the results of quantum transport, diffusive transport and collapse-resistant.

Corresponding Author: W.X. Zhang, E-mail address: wxzhang@chd.edu.cn and Z.Q. Shi, E-mail address: zhongqishi@mail.xjtu.edu.cn

1. Introduction

Indium Tin Oxide (ITO) is preferred to be used as the transparent conductor displays. The brittleness, inefficient processing, and high cost of ITO films have motivated a series of search for alternatives. Recently, copper NWs (Cu NWs) have attracted considerable interest due to great possible applications for a high-performance transparent conductor, which is inexpensive, flexible, can be deposited at low temperatures.¹ Moreover, copper exhibit unique structural and electrical properties as nanosized interconnects in microelectronics, which is one of the important characteristics for future microelectronic applications.²⁻⁹ Therefore, Cu NWs are low cost, flexible and have been extensively explored as an outstanding alternative, which will remove a significant barrier to the development of low-cost flexible displays, lighting, and solar cells.

After the realization of the fabrication NWs, the physical properties of Cu NWs are measured and calculated, especially their electron transport properties. Moreover, the bending effect on electronic transport in NWs is one of the important characteristics for its applications.⁶⁻⁹ When the length and width of Cu NWs are decreased to the mean free path of electrons, the mechanism of electronic transport changes to ballistic instead of diffusive. It is now known that the electric conductance is independent on the length of the NWs. The quantum conduction (G) is obtained from the Landauer formula and quantized in units of $G_0=2e^2/h$ where e denotes the electronic amount and h is the Planck constant.^{10,11} The ballistic transport properties of Cu NWs are influenced by atomic structures, size and stress.¹²⁻¹⁵ G of the pentagonal Cu NWs with [110] orientated structure is about $4.5G_0$ without bending stresses.¹⁰ When Cu NW is thin enough, it can turn into exotic structure rather than usual structure,¹⁶ which should be realized in nature.¹⁷ The quantum conductance of metallic nanowires is an exciting emerging field of both fundamental and applied relevance¹⁸⁻²⁰ since nanowires are building blocks for nanoelectronics^{21,22} and

nanoelectromechanical systems (NEMS).^{23,24} The stability and quantum conduction of both nonhelical and helical atomic Cu NW strands are reduced by applying a bending stress in our previous paper.^{25,26} In the service condition, the interconnect wire will be fixed on certain substrates, which may also induce strong stress field to the NWs. As we know, flexible displays and flexible solar cells frequently work in the circumstance of bending stress. Therefore, the effect of bending stress on G with different sizes, which is the precondition of the electronic transport in flexible displays and flexible solar cell, which is desirable to clarify systemically up to now.

In this contribution, we report an evolution of atomic, electronic structures and conduction properties of ultrathin Cu NWs under the coupling effect of size and bending stress. By the density functional theory (DFT) calculations, two different kind of atomic structures of Cu NWs with diameter from 0.2-1.0 nm are used. The density of states (DOS), $G(f)$ function and the electronic distribution are performed to determine changes of atomic and electronic structures of Cu NWs under bending stresses. It is found that the stability and quantum conduction of both nonhelical and helical atomic strands are reduced by applying a bending stress f . Moreover, as size of nanowires increases, the maximum bearable bending stress(f_c) decreases.

Based on DFT method, we have performed a systematic theoretical study of quantum conduction properties for seven kinds of different structure of copper nanowires. Furthermore, the electronic transport properties of Cu NWs between positive and negative electrodes could be implemented by means of DFTB method, which could not been achieved by DFT method.

2. Computational details

The first principles calculations have been performed within the framework of electronic density functional theory (DFT), as implemented in the DMOL³ model.²⁷ The generalized gradient approximation (GGA) functional with Perdew - Burke - Ernzerhof correlation gradient correction PBE method^{28,29} is employed to calculate transport properties of Cu NWs. The all-electron

relativistic^{30,31} is used for the core treatment. Our outlines of the used structures are directly obtained from the results of Wang *et. al.*³² The length of Cu NWs (L) is determined by the distance of the projection of mean locations of atom centers in the 1st and 20th layers along the axis. Brillouin zones (BZ) are sampled by a set of k -points grid ($5 \times 5 \times 1$) according to the Monkhorst-Pack scheme, which result in the convergence tolerance of energy of 2.0×10^{-5} Ha (1 Ha = 27.2114 eV), maximum force of 0.004 Ha/Å, and maximum displacement of 0.005 Å. V is directly applied along the axis of copper NW with values of 0.5 and 1 V/Å. The magnitude of $G(f)$ function of Cu NWs are decided by Landauer formula,⁵ which is reasonably valid in evaluating quantum transport for metallic wires. Based on the formalism, at zero Kelvin, G is given by

$$G = G_0 \sum_{i=1}^N T_i, \quad (1)$$

where T_i is the transmission probability of the i th channel and N is the number of propagating modes crossing Fermi energy (E_f). In case of perfect transmission in ballistic transport, no scattering is considered, namely, T_i is always unity. The layer electronic distributions within NWs are revealed by the Mulliken charge population.²⁵

The diffusive transport property of the Cu NWs are studied using the density-functional-based tight-binding (DFTB).³³⁻³⁵ DFTB is an approximation to DFT based on a second-order expansion of the DFT total energy around a reference electron density with significantly reduced computational cost. The matsci functional for Slater-Koster library method³⁶ is employed to calculate transport properties of Cu NWs. And the electrodes are considered to discover the different structures and diffusive transport properties of ultrathin Cu NWs by the effects of size and bending stress. Moreover, DFTB method would provide us a good opportunity to reveal the properties of large-scale nanowires in the future.

3. Results and discussion

Seven typical structures of Cu NWs obtained by the calculations are shown in Fig. 1. To characterize the structures of Cu nanowire, the notation $n_1-n_2-n_3-n_4$ ($n_1 > n_2 > n_3 > n_4$, from outer to inner) is introduced to describe a multi-shell nanowire consisting of coaxial tubes n_1 , n_2 , n_3 , n_4 atomic rows on each shell. n shows the atomic number of one atomic layer in the surface cell. Division as category, there are two different structures of Cu NWs where a represents a nonhelical strand and b is a helical one. Thus, the structures in Fig. 1(A) is defined as 3a, 3b, 4a, 4b and Fig. 1(B) is 6-1a, 6-1b, and 12-6-1, where 12 shows the atomic number of one atomic layer in the surface cell, 6 is in second-surface cell and 1 represents that in the core.³² The average stress strength f is obtained by averaging stress strength F of each layer according to our previous work.³⁷ According to the results of a genetic algorithm (GA) global search, there could be four possible structures of Cu NWs, non-compact nonhelical, compact nonhelical, left helical, and right helical, respectively.³² There is no difference on $G(f)$ functions is found in our simulation. Thus, the left helical direction is neglected in our simulation. Among these four structure, the non-compact nonhelical nanowire has higher energy than compact nonhelical wire, and the helical nanowire has the lowest energy. So In this contribution, the non-compact nonhelical is defined as a and right helical is defined as b, and the middle energy structures are neglected. These energy results are in good agreement with other computation results, which shows that the computation method is reliable.¹⁷ In general, the stable structure of Cu NWs is multi-shell packing composed of coaxial cylindrical shells or tubes. Each shell is formed by atom rows winding up helically side-by-side with different pitches of the helices, which have been theoretically predicted for Al and Pb NWs³⁸⁻⁴⁰ and experimentally observed in Au NWs.⁴¹

$L(f)$ results of seven structures are determined from Fig. 1 and showed in Table 1. When $f=0$, the distance between two neighboring layers at central axis (D) is always equals to 0.24 nm for 3a, 3b, 4a, 4b. Because the structures of 6-1a, 6-1b, 12-6-1 have the central axis atom, the value of $L(f=0)$ is different. Thus, $D \equiv 0.18$ nm for 6-1a, 6-1b, 12-6-1 in every layers. Once bending stress f is increasingly applied to Cu NWs, it is apparent that the length of the top layer atoms (L_{top}) for all

seven structures increases sharply, while the length of the down layer atoms (L_{down}) of nonhelical NWs decreases sharply in the same range. For example, when $f > 3$ nN, L_{top} of 3a decreases, while L_{down} of 3a keep constant. The reasons are as follows: Firstly, during the bending process, the top layer atoms are under tensile stress, while the down layer atoms are under compressive stress. Secondly, when $f > 3$ nN, the distances between certain atoms of the down layer are close to the critical value (0.23nm), and repulsive forces dominates the lattice distance. L_{down} of 3a has to keep constant because of insufficient space for the movement of atoms. In detail, with the increasing of bending stresses, the helical wire becomes disorder, suffering a phase transition to similar nonhelical one and collapsing eventually. The only difference between them is the critical value of 3b is 3.3nN while the value of 3a is 3nN. Moreover, when $f > 3$ nN for 3a and $f > 3.3$ nN for 3b, the stability of structure of Cu nanowire is broken and positions of atoms are out of order, and $L_{down}(f)$ keeps constant. The other structures have the similar situation. The multi-shell nanowire consisting of coaxial tubes, like as 6-1a, 6-1b and 12-6-1, exhibit comparative lower collapse-resistant f_c than other structures. For 3a, 3b, 4a, 4b, there is no atom in the core, which is difficult to move into other layers, and the distance between every layer reduces hardly. Thus, the collapse-resistant f_c are 3nN, 3.3 nN, 2.8 nN, 3.1nN, 2.5nN, 3nN and 2 nN for 3a, 3b, 4a, 4b, 6-1a, 6-1b and 12-6-1, respectively.

As f increases, the corresponding results of D are shown in Table 1. For example, for 4b, when $f=3.1$ nN, $D_{2-3} = 0.28$ nm, $D_{17-18} = 0.28$ nm. When $f=3.3$ nN, $D_{2-3} = 0.39$ nm, $D_{17-18} = 0.42$ nm, where the subscript numbers denote the corresponding layer numbers. As D_{4-6} increases, due to the nature of ballistic transport, the probability of electron jump between the two layers decreases and thus G decreases. The atoms in the odd layer move toward the directions of both tips of the structure. Thus, $D_{2-3}(f=3.1$ nN) is about 1.17 times of that for 4b at $f = 0$. Moreover, there are similar situation for the other structures, the value of D_c (f_c) for all seven structures are about 1.10-1.25 times of that at $f = 0$, which is only dependent on f but independent on the nanowire diameter (d). The larger value of D_{2-3} is induced by the atomic movement of the atom in the 3th layer putting into the 4th layer.

The magnitude of G or the conduction channels is decided by the number of bands crossing Fermi level E_F on the basis of the Landauer formula.⁹ The calculated $G(f)$ values of seven structures with all conduction channels are shown in Fig. 2 and Table 2. For NWs with the same size, the energy bands at the vicinity of Fermi level and the number of conduction bands crossing the Fermi level are determined by the atomic configuration of different isomers. Namely, $G(f)$ sensitively depends on the atomic structures of the wires. 4a Cu NWs has four ballistic conduction channels, whereas 4b has three channels. Thus, $G(f=0) = 3$ for 4a, which agrees with other results.¹⁷ As f increases to 2.8 nN, $G(f=2.5\text{nN})/G(f=0) = 1$ for 4a, which means the structure still stable under relatively weak bending stress. However, $G(f=2.8\text{nN})/G(f=0) = 0.6667$, the structure is unstable under relatively large bending stress. On the other hand, 4b Cu NWs has the similar situation. Hence, $G(f)$ functions of the structures indeed have opposite tendencies on $L_{top}(f)$ before their structures collapse. It is because that the atom accumulation becomes weaker when the distance among some atoms increases.¹⁹ For 4a, $L_{top}(f=2.5\text{nN})$ reaches the maximum value where the atomic structure varies and distance between layers (D) in the middle of 4a increases. As D_{18-19} increases, due to the nature of ballistic transport, the probability of electron jump between the two layers decreases and thus G decreases.

Similar to 4a, when $0 < f < 3.1\text{nN}$, $L_{down}(f)$ functions of 4b drop monotonously, while $D(f)$ of the middle layers increase a little. Because of the evident decreasing of $D_{down1-8}$ and $D_{down13-20}$, L_{down} drops from 4.56 to 4.18 nm at $f=3.1\text{ nN}$. When $f=3.3\text{ nN}$, the structure collapses and G decreases to zero while $L_{down}(f)$ keeps constant. It means that the critical collapse-resistant f_c of 4b is higher than $f_c = 2.8\text{ nN}$ of 4a. 4b could stand higher bending stress than 4a and would collapse under higher force intensity. These results are in agreement with the results of structures analyses.

When the wire diameter of Cu NWs (d) is constant, $G(f)$ of helical NWs and nonhelical NWs decrease. As $f=0$, G (in unit of G_0) approximately fit into a quadratic function of d (in unit of Å) as:³²

$$G(f=0) = 2.0 + 0.12 \times d^2. \quad (2).$$

This is easily understandable since d^2 gives the area of the cross section of the NWs. As shown in Table 2, when $f > 0$, G could be also approximately fitted into the following function, and we also can find the relationship between $G(f_c)$ vs d as:

$$G(f_c) = 5.55 - 14.73 \times d + 17.36 \times d^2 \quad \text{for nonhelical NWs} \quad (3)$$

$$G(f_c) = 3.67 - 1.755 \times d \quad \text{for helical NWs} \quad (4)$$

This means that the bending stress effect of nonhelical NWs on $G(f_c)$ is decided by the cross section area while the bending stress effect of helical NWs on $G(f_c)$ is decided by the diameter.

DOS of the seven structures observed by DFT are present in Fig. 2. For all the seven structures, once f is applied, the position of largest peak shifts rightward. When Cu nanowire collapses, the largest peak obviously shifts left, and the largest peak of DOS below E_f is located between -1.89 and 0.67 eV under $f = 0$, while -2.27 and -0.09 eV under $f = 2.8$ nN. The case is similar for other structures, which implies the energy of all structures increase. It implies that the energy of all the structures are separated into two or three pieces. Considering the movement of the maximum peak, the energy of all the structures increases firstly, and then goes down when the collapse occurs. It is because that the original stable structures will be transferred to unstable structures when the bending stress is considered. When Cu nanowire collapses, the effect of collapse-resistant disappears, which results in the decrease of energy. For 4a, the magnitude of DOS at E_f under $f = 2.8$ nN decreases to 0.5 times of that under $f = 0$. As f further increased to 3 nN, with the collapse of the structure, the magnitude of DOS at E_f decreases to 0. Under $f = 3.1$ nN, the value for 4b is 0.5 times of that under $f = 0$. In the same way, the above results of DOS ratios at E_f confirm the calculated results $G(f_c)$ from Landauer formula⁴² shown in Figs. 2(a), (b), (c), and (d), where the corresponding $G(f_c)$ ratios are about 0.5 for seven structures.

Mullikan charge $e(f)$ functions of all structures are shown in Fig. 3. And the indexed layer is the same as in Fig. 1. Under $f = 0$, the sum total of e of all layers is 0 for all seven structures. $e(f)$ functions of 6-1a and 6-1b are shown in Figs. 3(a) and (b). In Fig. 3(a), as $f = 1.5$ nN, although the charge distribution of 6-1a has been a little different with under $f = 0$, the positive and negative

charges are still in sequence. There is no influence on the electronic transport. However, when f increases to 2.5 nN, the distribution of charge is totally changed, which leads to the electron accumulation. This accumulation could induce the decrease of G and then affect the electronic transport properties of Cu NWs. While f further increases to 2.8 nN, the distribution of charge is no longer symmetric and in disorder.¹⁸ The electrons transport is destroyed and the electron is accumulated in the 6th and 14th layers.

In the case of 6-1b, electrons are equally distributed in all layers when $f = 0$. The positive and negative charges are alternately distributed and have the same absolute value. However, when $0 < f < 3$ nN, the distribution of charges along the axes are inhomogeneous and has been obviously changed. But absolute value of all layers is no longer consistent. And the positive and negative charges are still alternately distributed, which is no influence on the electronic transport. Moreover, as f further increases, the inhomogeneous distribution of the charge is more obvious. Once f is equal to 3 nN, a new layer consisting of seven Cu atoms is combined and formed by some of the odd and even layers. Thus, the channel numbers of ballistic transport are increased by the new layer. At the same time, the channel numbers of the neighboring layer have been decreases. When f further increases to 3.2 nN, the total energy decreases and the structure trends to be more stable. The above so-called new layer further generates, which it is unfavorable to electronic transport. The distribution of charge is dissymmetric and disorder. The electrons transport is broken off and the electron also accumulates in the 12th layers, just like the results of 6-1a under $f = 2.8$ nN.

Electronic transmission properties for the seven structures are observed by DFTB and presented in Fig. 4. When $f = 0$, the electronic transmission properties for 6-1a, 6-1b and 12-6-1 are almost symmetrical, while the electronic transmission properties for 3a, 3b, 4a and 4b are completely asymmetric. The asymmetric transmission properties are not beneficial to the diffusive transport properties. Once the electrode reverses, only symmetric system could achieve favorable conduction properties. There are no intermediary atoms for the structure of 3a, 3b, 4a and 4b, which induce that the positive ions can't pass through in the middle layer under the effect of electrodes,

and the asymmetry of transmission properties. For 3a and 3b, when $f > 0$, there are still no intermediary atoms appearing in the bending process, and thus, the asymmetry of transmission properties still are unchanged. For 4a and 4b, when $f = 2.8$ nN for 4a and $f = 3.1$ nN for 4b, the symmetry of transmission performances are apparently improved, which are induced by some intermediary atoms appearing in the bending process. Furthermore, for 6-1a, 6-1b and 12-6-1, when $f > 0$, the symmetry of transmission performances fall slightly down. When $f = f_c$ for seven structures, the symmetry of transmission performances are completely disappeared, which means that the diffusive transport properties for the three structures of 6-1a, 6-1b and 12-6-1 vanished as the structures collapse. It is in reasonable agreement with the DFT results above in the bending process.

Electron potential results of the seven structures are observed by DFTB and presented in Fig. 5. When $f = 0$, taking 12-6-1 as an example according to the figure of electron potential, the negative potential (red) on the surface of Cu nanowire, the positive potential (blue) in the central region, a loop is formed between two electrodes. Therefore, the intermediary atoms are the highlight to form the loop and implement diffusion transport. Similarly for all the seven structures, when $f = 0$, 6-1a, 6-1b and 12-6-1 have the positive potential (blue) in Fig. 5, while 3a, 3b, 4a and 4b don't have the positive potential. Combination with Fig. 4, we can come to the conclusion that due to no intermediary atoms, there are no diffusive properties for 3a, 3b, 4a, 4b when $f = 0$. When $f = 2.8$ nN for 4a and $f = 3.1$ nN for 4b, there are some intermediary atoms in the bending process, and then the loops for the systems have formed. But a lot of the potential energy are gathering in the middle region of nanowire leading to the decrease of the diffusive transport properties. When $f > 0$, for 6-1a, 6-1b and 12-6-1, the positive potentials slightly fall down. When $f = f_c$ for seven structures, the positive potentials are all disappeared when the structures collapse. Excellent agreements are observed among the electron potential results, DFT results and electronic transmission properties above. It can easily come to the result that 6-1a, 6-1b and 12-6-1 express better diffusive transport properties than other structures (3a, 3b, 4a and 4b). 6-1b ultrathin Cu NWs exhibits the best properties by comprehensively considering the results of quantum transport, diffusive transport and

collapse-resistant.

4. Conclusion

In summary, the first-principle calculations are performed to investigate the effect of bending stress on the stability and ballistic transport properties of Cu NWs with diameter from 0.2-1.0 nm. From the details that mentioned above, we can to the following conclusions. (1) Without bending stress, the conduction of Cu NWs generally increases with the increasing of its diameter. (2) When the bending stress is considered, all of nonhelical and helical structures are more unstable; the helical atomic strands are more stable than the nonhelical ones since the former owns higher collapse-resistant f_c . (3) $G(f_c)$ is decided by the area of the cross section of nonhelical NWs, while decided by the diameter of helical NWs. $G(f)$ function decreases as f increases when $0 < f < f_c$. When f is above f_c , $G(f)$ is decreased to zero for all seven structures. (4) The intermediary atoms are the highlight to form the loop between two electrodes and implement diffusion transport for the ultrathin Cu NWs. (5) 6-1a, 6-1b and 12-6-1 have better diffusive transport properties than 3a, 3b, 4a and 4b according to the results of DFTB. Among the seven structures, 6-1b exhibits the best properties by comprehensively considering the results of quantum transport, diffusive transport and collapse-resistant.

Acknowledgements.

The authors acknowledge supports by National Key Basic Research and Development Program (2012CB619400), National Natural Science Foundation of China (NSFC, Grant Nos. 51471124 and 51301020), Natural Science Foundation of Shaanxi province, China (2014JQ6196), Ph.D. Programs Foundation of Ministry of Education of China (Grant No. 20110201120002), the special fund for basic scientific research of central colleges of Chang'an University (No. 2013G1311053) and State Key Laboratory for Mechanical Behavior of Materials.

Reference

- 1 A. R. Rathmell, S. M. Bergin, Y. L. Hua, Z. Y. Li, and B. J. Wiley, *Adv Mater.* 2010, **22**, 3558.
- 2 Q. Q. Dai, Y. F. Zhu, and Q. Jiang, *Phys. Chem. Chem. Phys.* 2012, **14**, 1253.
- 3 Z. Q. Shi, Z. L. Wei, C. He, R. F. Jing, H. J. Wang and G. J. Qiao, *RSC Adv.* 2014, **4**, 62926.
- 4 R. Basori, K. Das, P. Kumar, K. S. Narayan, A. K. Raychaudhuri, *Appl. Phys. Lett.* 2013, **102**, 061111.
- 5 L. Q. Li, Z. F. Liu, M. Li, L. Hong, H. Shen, C. L. Liang, H. Huang, D. Jiang, S. Ren, *J. Phys. Chem. C* 2013, **117**, 4253.
- 6 Y. F. Zhu, X. Y. Lang, W. T. Zheng. Lian and Q. Jiang, *ACS Nano* 2010, **4**, 3781.
- 7 S. Monti, C. Li, V. Carravetta, *J. Phys. Chem. C* 2013, **117**, 5221.
- 8 B. Weber, S. Mahapatra, H. Ryu, S. Lee, A. Fuhrer, T. C. G. Reusch, D. L. Thompson, W. C. T. Lee, G. Klimeck, L. C. L. Hollenberg, *Science* 2012, **335**, 64.
- 9 G. A. Gelves, B. Lin, U. Sundararaj, and J. A. Haber, *Adv. Funct. Mater.* 2006, **16**, 2423.
- 10 L. Olesen, E. Laegsgaard, I. Stensgaard, F. Besenbacher, J. Schiøtz, P. Stoltze, K. W. Jacobsen, and J. K. Nørskov, *Phys. Rev. Lett.* 1994, **72**, 2251.
- 11 X. Zhang, J. L. Kuo, M. Gu, X. Fan, P. Bai, Q. G. Song, C. Q. Sun, *Nanoscale* 2010, **2**, 412.
- 12 Q. G. Jiang, Z. M. Ao and Q. Jiang, *Phys. Chem. Chem. Phys.* 2013, **15**, 10859
- 13 G. E. Tommei, F. Baletto, R. Ferrando, R. Spadacini, and A. Danani, *Phys. Rev. B* **69**, 2004, 115426.
- 14 J. J. Zhao, C. Bui, J. Han, and J. P. Lu, *Nanotechnology* 2003, **14**, 501.
- 15 C. Q. Sun, H. L. Bai, S. Li, B. K. Tay, C. Li, T. P. Chen, and E. Y. Jiang, *J. Phys. Chem. B* 2004, **108**, 2162.
- 16 E. Tosatti, S. Prestipino, S. Kostlmeier, A. Dal Corso, and F. D. Di Tolla, *Science* 2001, **291**, 288.
- 17 O. Gulseren, F. Ercolessi, and E. Tosatti, *Phys. Rev. Lett.* 1998, **80** 3775.
- 18 C. J. Muller, J. M. vanRuitenbeek, and L. J. deJongh, *Phys. Rev. Lett.* 1992, **69**, 140.
- 19 U. Landman, W. D. Luedtke, B. E. Salisbury, and R. L. Whetten, *Phys. Rev. Lett.* 1996, **77**, 1362.
- 20 W. A. De Heer, S. Frank, and D. Ugart, *Zeits. Phys. B* 1997, **104**, 469.
- 21 N. Agrait, A. L. Yeyati, and J. M. van Ruitenbeek, *Phys. Rep.* 2003, **377**, 81.
- 22 D. R. Bowler, *J. Phys.: Condens. Matter* 2004, **16**, R721.
- 23 M. D. Ventra, S. Evoy, and J. R. Heflin, Introduction to Nanoscale Science and Technology

- (Boston, MA: Kluwer Academic), (2004).
- 24 X. Q. Zhang, H. Li and K. M. Liew, *Journal of Applied Physics* 2007, **102**, 073709.
 - 25 C. He, W. X. Zhang, Z. Q. Shi, J. P. Wang, and H. Pan. *Appl. Phys. Lett.* 2012, **100**, 123107.
 - 26 C. He, W. X. Zhang, J. L. Deng, *J. Phys. Chem. C* 2011, **115**, 3327.
 - 27 B. Delley, *J. Chem. Phys.* 2000, **113**, 7756.
 - 28 J. W. Zhu, D. N. Shi, J. J. Zhao, and B. L. Wang, *Nanotechnology* 2010, **21**, 185703.
 - 29 J. P. Perdew, K. Burke, and M. Ernzerhof, *Phys. Rev. Lett.* 1996, **77**, 3865.
 - 30 Y. F. Zhu, Q. Q. Dai, M. Zhao and Q. Jiang, *Sci. Rep.* 2013, **3** 1524.
 - 31 Z. M. Ao, and F. M. Peeters, *Appl. Phys. Lett.* 2010, **96**, 253106.
 - 32 B. L. Wang, J. J. Zhao, X. S. Chen, D. Shi, and G. H. Wang, *Nanotechnology* 2006, **17**, 3178.
 - 33 G. Seifert, D. Porezag, and T. Frauenheim, *Int. J. Quantum Chem.* 1996, **217**, 502.
 - 34 D. Porezag, T. Frauenheim, T. Kohler, G. Seifert, and R. Kaschner, *Phys. Rev. B* 1995, **51** 12947.
 - 35 M. Elstener, D. Porezag, G. Jungnickel, J. Elsner M. Haugk T. Frauenheim, S. Suhai and G. Seifert *Phys. Rev. B* 1998, **58** 7260.
 - 36 R. Luschtinetz, J. Frenzel, T. Milek, and G. Seifert, *J. Phys. Chem. C*, 2009, **113**, 5730.
 - 37 C. He, L. Qi, W. X. Zhang, and H. Pan. *Appl. Phys. Lett.* 2011, **99**, 073105.
 - 38 B. L. Wang, S. Y. Yin, G. H. Wang, J. J. Zhao, *J. Phys.: Condens. Matter*, 2001, **13**, L403.
 - 39 B. L. Wang, G. H. Wang, J. J. Zhao, *Phys. Rev. B* 2002, **65**, 235406.
 - 40 A. J. Simbeck, N. Lanzillo, N. Kharche, M. J. Verstraete, S. K. Nayak, *ACS Nano* 2012, **6**, 10449.
 - 41 Y. Kondo, K. Takayanagi, *Science* 2000, **289**, 606.
 - 42 D. Liu, J. S. Lian, Q. Jiang, *J. Phys. Chem. C* 2009, **113**, 1168.

TABLE 1. Part critical data of length (L) and the distance between two neighboring layers at central axis (D) in the calculations under f . When $f=0$, $L\equiv 4.56\text{nm}$ and $D\equiv 0.24\text{ nm}$ for 3a, 3b, 4b, while $L\equiv 3.42\text{nm}$ and $D\equiv 0.18\text{ nm}$ for 6-1a, 6-1b, 12-6-1 in every layers.

Wire, f	D_{2-3}	D_{3-4}	D_{11-12}	D_{14-15}	D_{15-16}	D_{17-18}	D_{19-20}	L
3a, 3nN	0.24	0.24	0.24	0.26	0.30	0.24	0.32	4.52
3a, 3.2nN	0.24	0.24	0.23	0.33	0.36	0.26	0.34	4.60
3b, 3.3nN	0.25	0.26	0.23	0.25	0.25	0.24	0.26	4.48
3b, 3.5nN	0.25	0.38	0.23	0.24	0.24	0.28	0.32	4.53
4a, 2.8nN	0.26	0.24	0.23	0.25	0.24	0.25	0.26	4.42
4a, 3nN	0.30	0.26	0.24	0.24	0.24	0.32	0.30	4.49
4b, 3.1nN	0.28	0.25	0.23	0.24	0.24	0.28	0.26	4.45
4b, 3.3nN	0.39	0.27	0.23	0.24	0.24	0.42	0.29	4.50
6-1a, 2.5nN	0.19	0.19	0.17	0.22	0.23	0.20	0.18	3.36
6-1a, 2.8nN	0.12	0.16	0.16	0.20	0.32	0.16	0.15	3.39
6-1b, 3 nN	0.08	0.11	0.20	0.18	0.18	0.12	0.13	3.38
6-1b, 3.2nN	0.18	0.18	0.38	0.26	0.16	0.12	0.13	3.39
12-6-1, 2nN	0.17	0.16	0.16	0.15	0.16	0.17	0.16	3.41
12-6-1, 2.2nN	0.16	0.22	0.16	0.15	0.24	0.36	0.16	3.44

TABLE 2. The diameter (d), $G(f)$ function of Cu NWs obtained from DFT calculations. d in nm. G in G_0 . f in nN.

Wire	d	$f=0$	$f=2.0$	$f=2.2$	$f=2.5$	$f=2.8$	$f=3$	$f=3.1$	$f=3.2$	$f=3.3$	$f=3.5$
3a	0.242	3	3	3	3	3	2	0	0	0	0
3b	0.212	2	2	2	2	2	2	2	2	1	0
4a	0.277	4	4	4	4	2	0	0	0	0	0
4b	0.288	3	3	3	3	3	3	2	0	0	0
6-1a	0.490	4	4	4	2	0	0	0	0	0	0
6-1b	0.418	4	4	4	4	4	2	0	0	0	0
12-6-1	0.942	12	4	0	0	0	0	0	0	0	0

Captions

Fig. 1 Morphologies of Cu NWs as a function of f . The average stress strength f is obtained by averaging stress strength F of each layer. f in nN. 3a, 3b, 4a, 4b are shown in (A) and 6-1a, 6-1b, 12-6-1 are shown in (B) can be shown as.

Fig. 2 G , DOS of nonhelical NWs of 3a, 4a, 6-1a and helical NWs of 3b, 4b, 6-1b, 12-6-1 as a function of f . $E_f = 0$ (vertical dotted line) is taken.

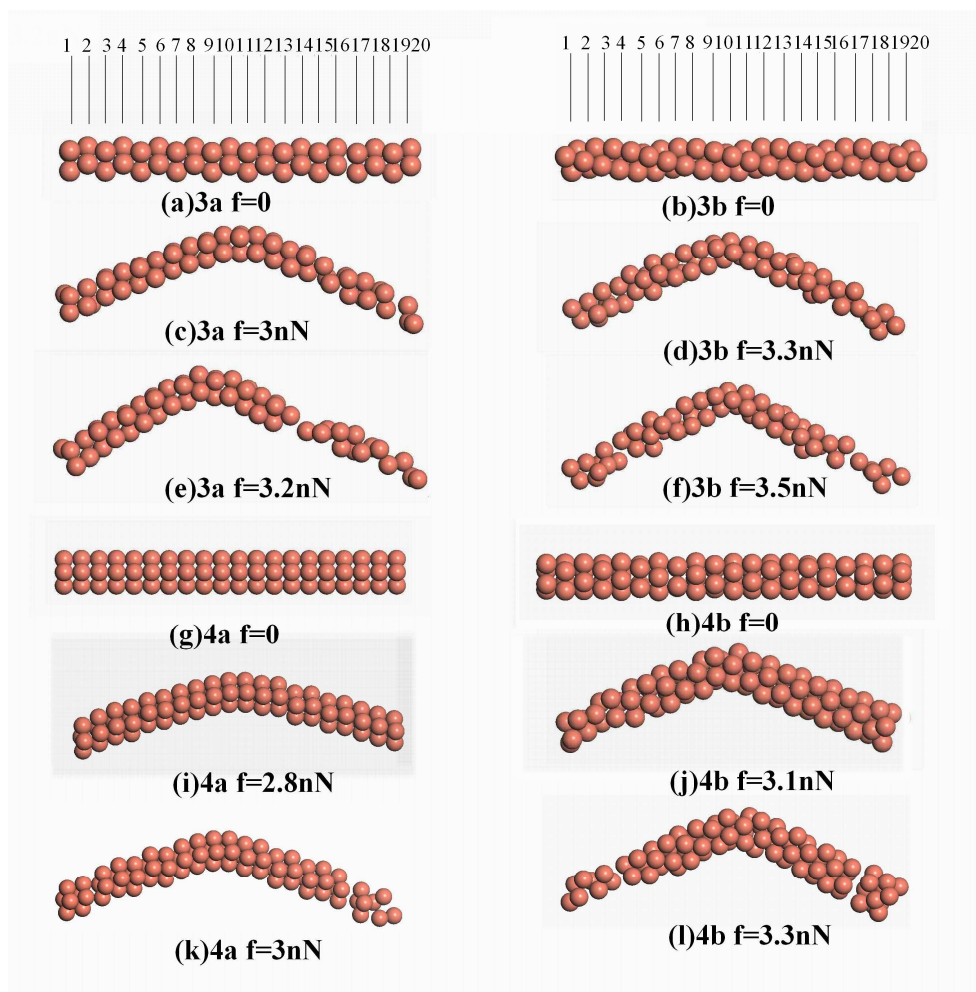
Fig. 3 The Mulliken charge population of nonhelical NWs of 3a, 4a, 6-1a and helical NWs of 3b, 4b, 6-1b, 12-6-1. The charges show the sum of each layer and the layer number is defined in Fig. 1.

Fig. 4 Electronic transmission properties of the seven structures observed by DFTB.

Fig. 5 Electron potential of the seven structures observed by DFTB, where red is negative potential and blue is positive potential.

Fig. 1

(A)



(B)

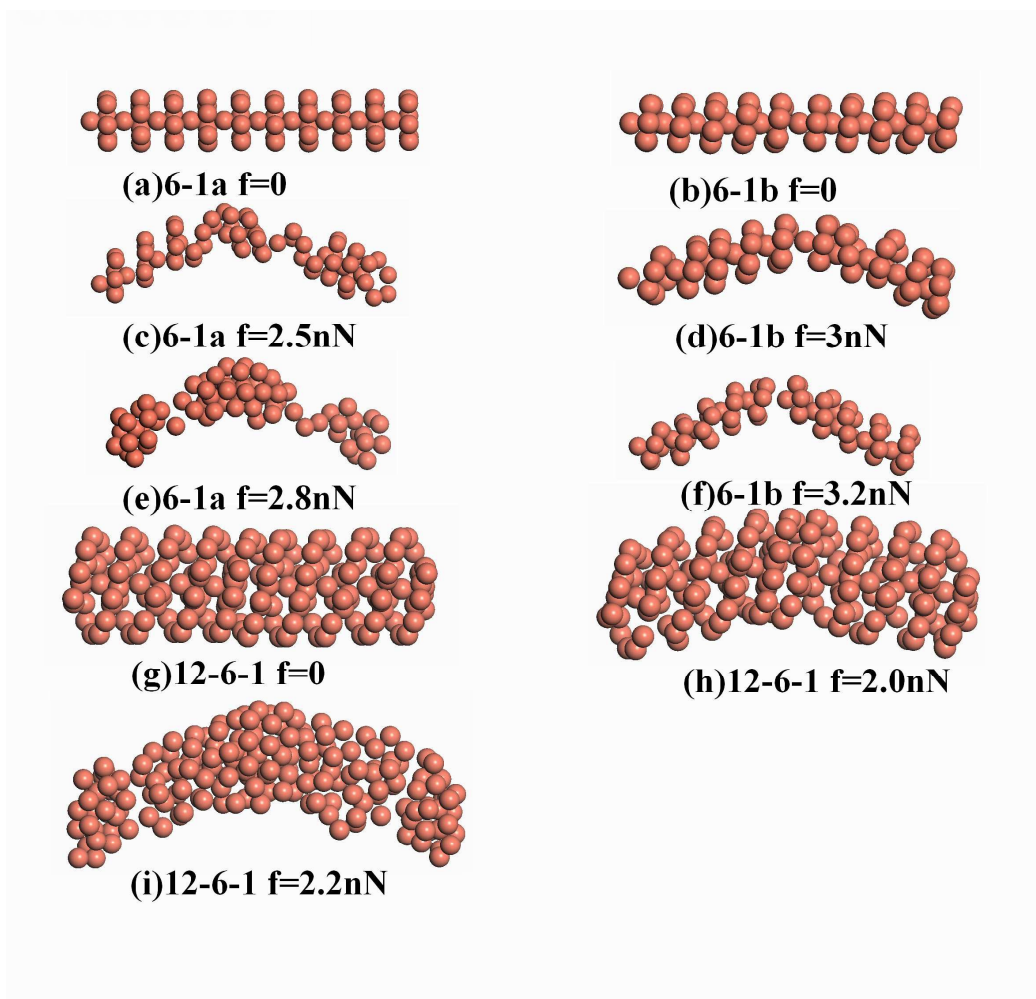
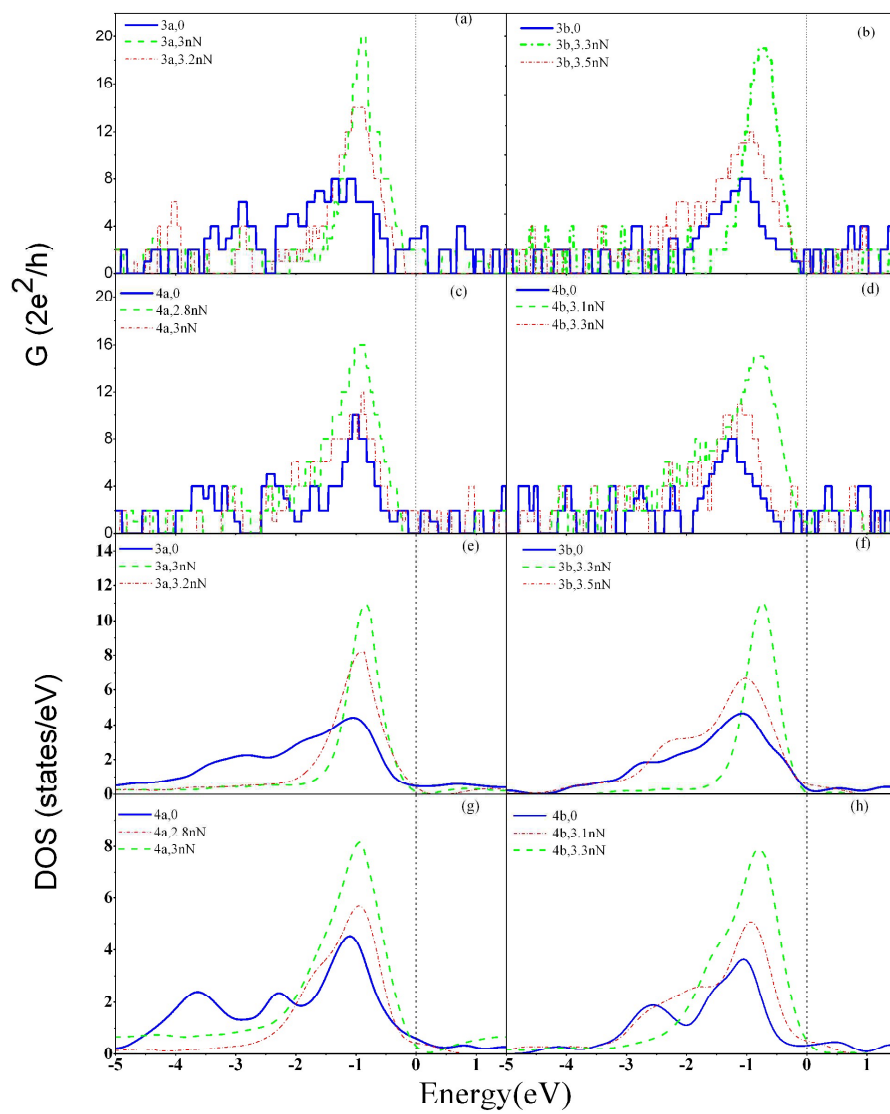


Fig. 2

(A)



(B)

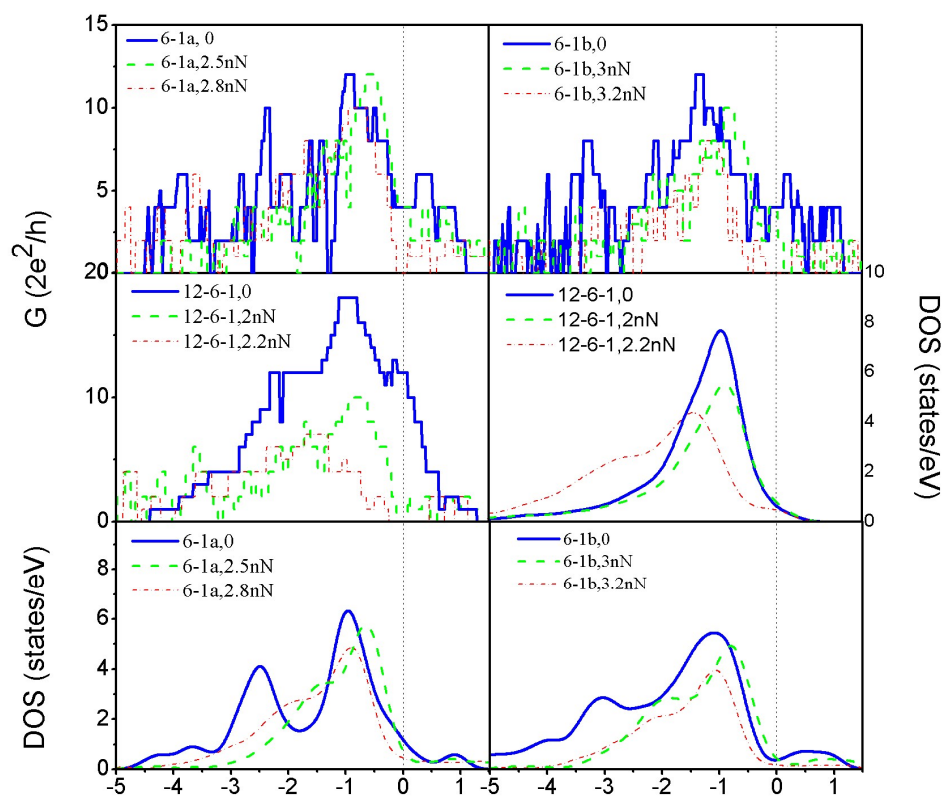


Fig. 3

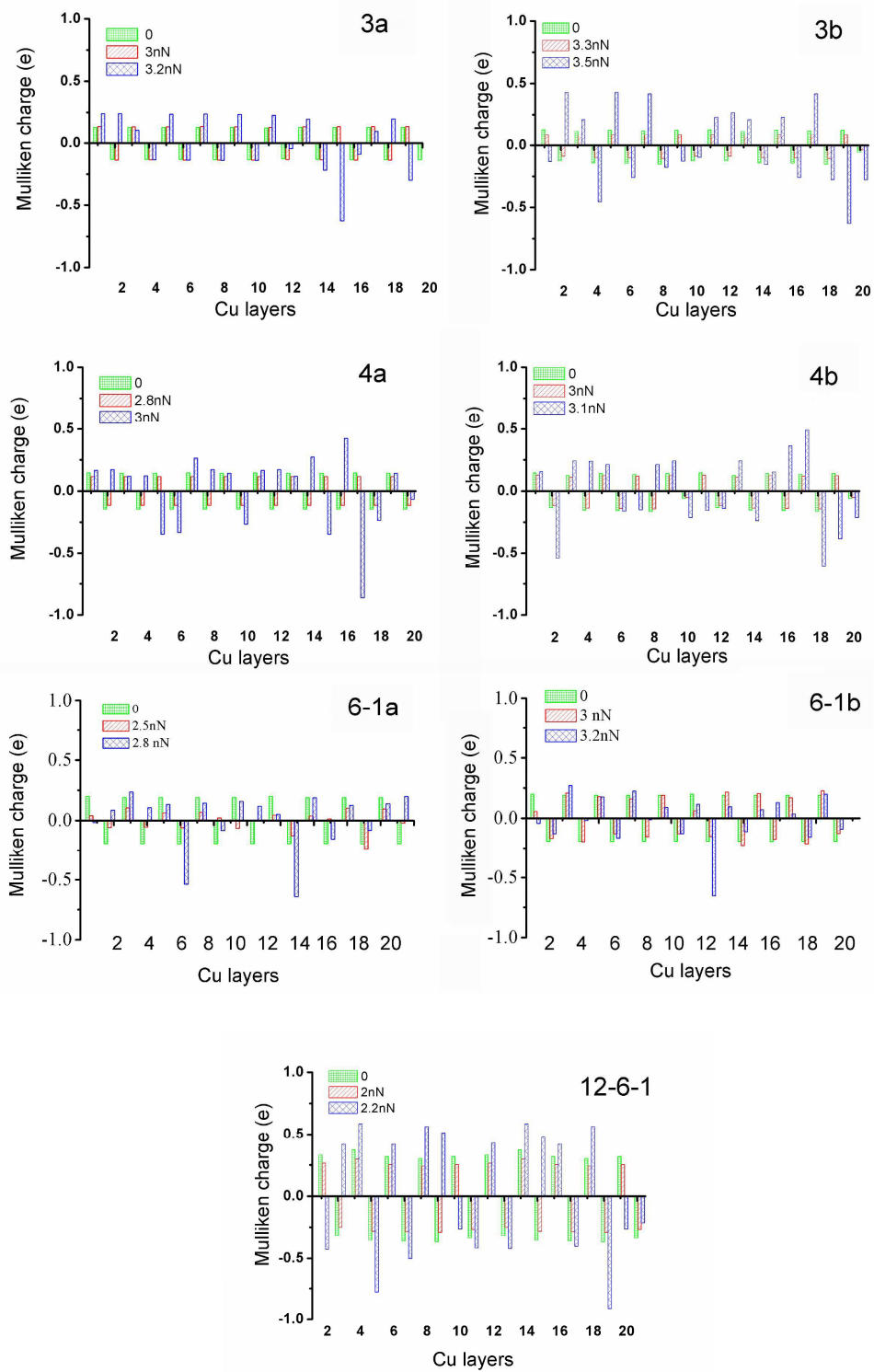


Fig. 4

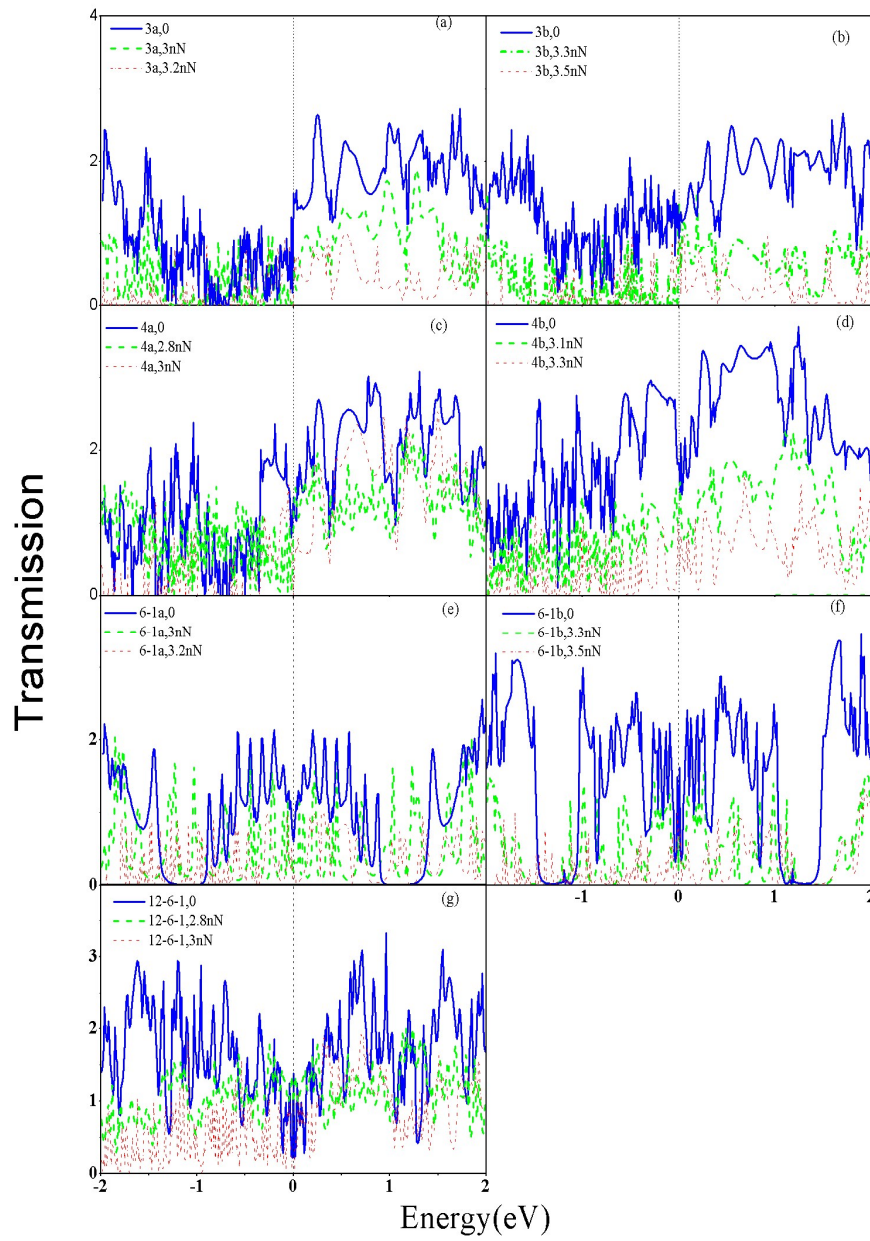
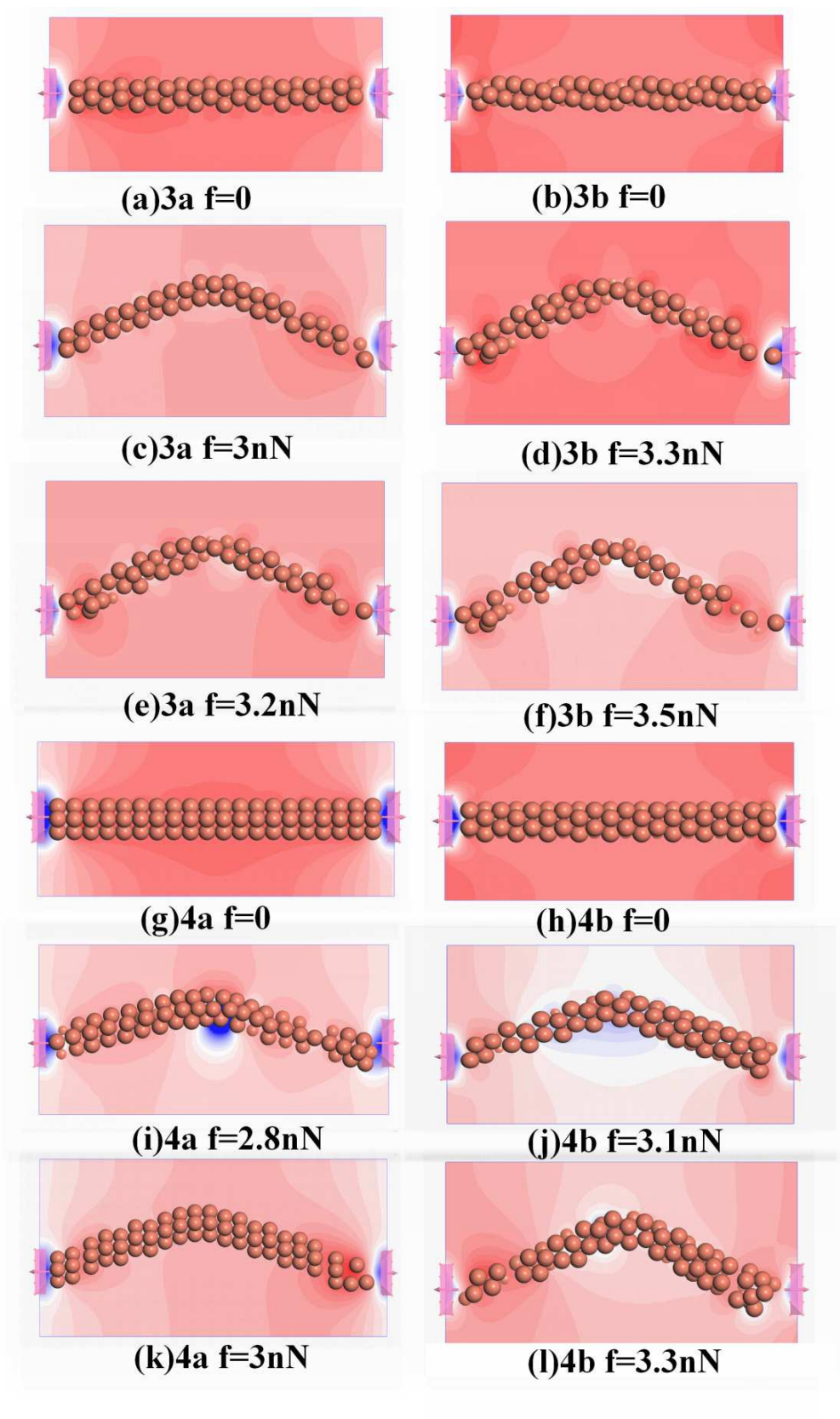
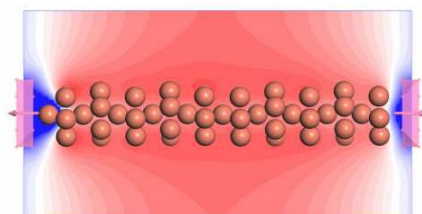
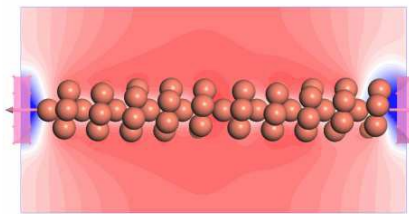
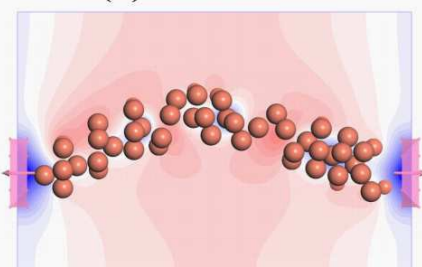
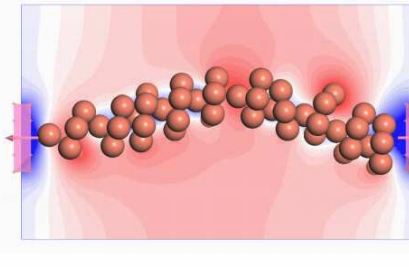
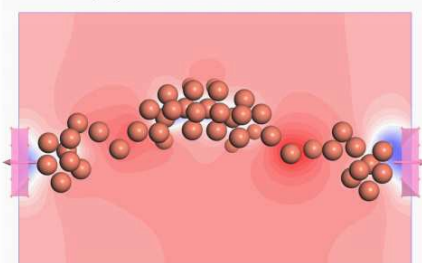
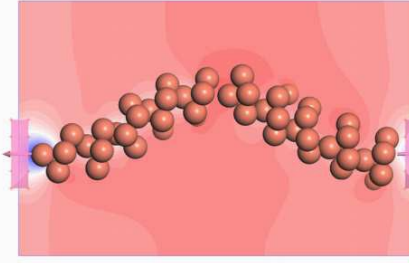
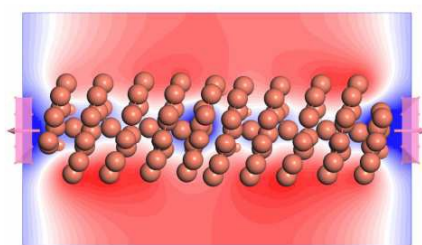
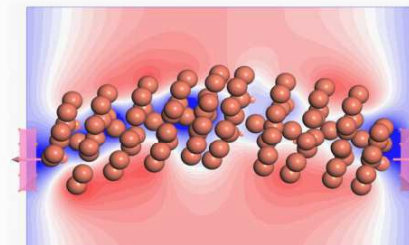
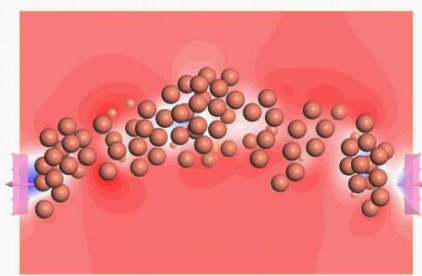


Fig. 5
(A)

(B)

**(a)6-1a $f=0$** **(b)6-1b $f=0$** **(c)6-1a $f=2.5\text{nN}$** **(d)6-1b $f=3\text{nN}$** **(e)6-1a $f=2.8\text{nN}$** **(f)6-1b $f=3.2\text{nN}$** **(g)12-6-1 $f=0$** **(h)12-6-1 $f=2.0\text{nN}$** **(i)12-6-1 $f=2.2\text{nN}$**

The electron transport properties of ultrathin Cu nanowires (NWs) with diameter of 0.2-1.0 nm under different bending stresses are reported for the future application in flexible displays and flexible solar cell. The density functional theory (DFT) and density-functional-based tight-binding (DFTB) approaches have been combined to systematically discover the ballistic transport and diffusive transport of ultrathin Cu NWs in the nanoscale. Our DFT calculations show that as the size of nanowires increases, the maximum bearable bending stress (f_c) reduces. Our DFTB calculations reveal that the intermediary atoms are the highlight to form the loop between two electrodes and implement diffusion transport. Among the seven structures, the 6-1b exhibits the best properties by comprehensively considering the results of quantum transport, diffusive transport and collapse-resistant.

